ADVANCED FUNCTIONAL MATERIALS
www.afm-journal.de

Multi-Color 3D Printing via Single-Vat Grayscale Digital Light Processing

*Xirui Peng, Liang Yue, Sizhuang Liang, Stuart Montgomery, Chunliang Lu, Chieh-Min Cheng, Raheem Beyah, Ruike Renee Zhao, and H. Jerry Qi**

Digital light processing (DLP) is a high-resolution, high-speed additive manufacturing method that builds 3D parts by selectively curing photopolymerizable resins layer-by-layer. To achieve multi-color DLP printing, researchers have used multiple switchable resin vats. However, these methods require complex vat switching devices and cleaning manipulations, leading to low efficiency. Therefore, it remains a challenge to achieve multi-color DLP 3D printing efficiently. In this study, a single-vat multi-color DLP 3D printing by using an anthraquinone-based dye is realized. The dye can be oxidized by the free radicals released from photoinitiators under ultraviolet light and change the color from blue to yellow. This color-changing mechanism permits a graded spectrum of colors as concomitants of the photopolymerization process during DLP printing by controlling the light dose without using extra vats or devices. Multi-color demonstrations, such as engineering stress simulation results in 3D and multi-color vases, are successfully fabricated, showing great versatility and efficiency.

1. Introduction

3D printing, or additive manufacturing, has elicited extensive attention and numerous research efforts in recent years.[1–3] Compared to the traditional manufacturing method, 3D printing builds parts layer-by-layer, lending itself the capability to create complicated structures and customizable articles. With the development of 3D printing techniques and printable materials, more advanced applications have been demonstrated in a variety of areas, including 4D printing,[4–9] metamaterials,[10–12] biomedicine,[13–15] and electronics.[16–18]

One of the most promising 3D printing techniques is digital light processing (DLP), which uses a ultraviolet (UV) projector to selectively cure photopolymerizable resins in a vat with 2D patterns (**Figure 1**a). After the light exposure, the liquid resin solidifies to a layer of the polymer. By repeating this process, 3D parts can be formed by the accumulation of a series of 2D layers. DLP has advantages of high printing resolution and speed. First, the resolution of DLP 3D printing is determined by the pixel size of the projector for in-plane and the minimum step of the Z-stage motor in the z-direction, both of which typically range from 20 to 100 μm. Second, since an entire layer is formed at a time (typically a few seconds), DLP prints much faster than extrusion-based methods that employ a "line-by-line then layer-by-layer" approach. Recently, the continuous liquid interface production (CLIP),[19] a DLP-based method, has reached a higher speed up to 500 mm h^{-1} by using an oxygen-permeable film that creates a dead zone between the transparent bottom and liquid resin, which enables continuous layerless fabrication. Moreover, the high-area rapid printing (HARP)[20] breaks the thermal limitations on the printbed size with a mobile liquid interface (flowing immiscible fluorinated oil), which can dissipate heat and minimize interfacial adhesion at the build region, and achieved a volumetric throughput of 100 L h^{-1}.

However, despite these advantages, the direct incorporation of multiple colors into DLP printed parts is still a challenge. Printing colorful articles are important in 3D printing, since colors not only provide visual effects that delight people but also serve as the media to store and convey information.[21] Thus, driven by the aesthetic and informative significance, post-processing steps, such as coating, painting, and functionalization, are typically adopted to impart colors to the printed parts.[22–26] Alternatively, multi-material 3D printing[27–30] or materials with tunable colors[31] can be utilized to directly print multi-color articles. This is relatively easier for extrusion-based and

X. Peng, L. Yue, S. Montgomery, H. J. Qi
The George W. Woodruff School of Mechanical Engineering
Georgia Institute of Technology
Atlanta, GA 30332, USA
E-mail: qih@me.gatech.edu
X. Peng, H. J. Qi
Renewable Bioproduct Institute
Georgia Institute of Technology
Atlanta, GA 30332, USA
S. Liang, R. Beyah
The School of Electrical and Computer Engineering
Georgia Institute of Technology
Atlanta, GA 30332, USA
C. Lu, C.-M. Cheng
Technology and Development Group
Xerox Corporation
Webster, NY 14580, USA
R. R. Zhao
Department of Mechanical Engineering
Stanford University
Stanford, CA 94305, USA

The ORCID identification number(s) for the author(s) of this article can be found under https://doi.org/10.1002/adfm.202112329.

DOI: 10.1002/adfm.202112329

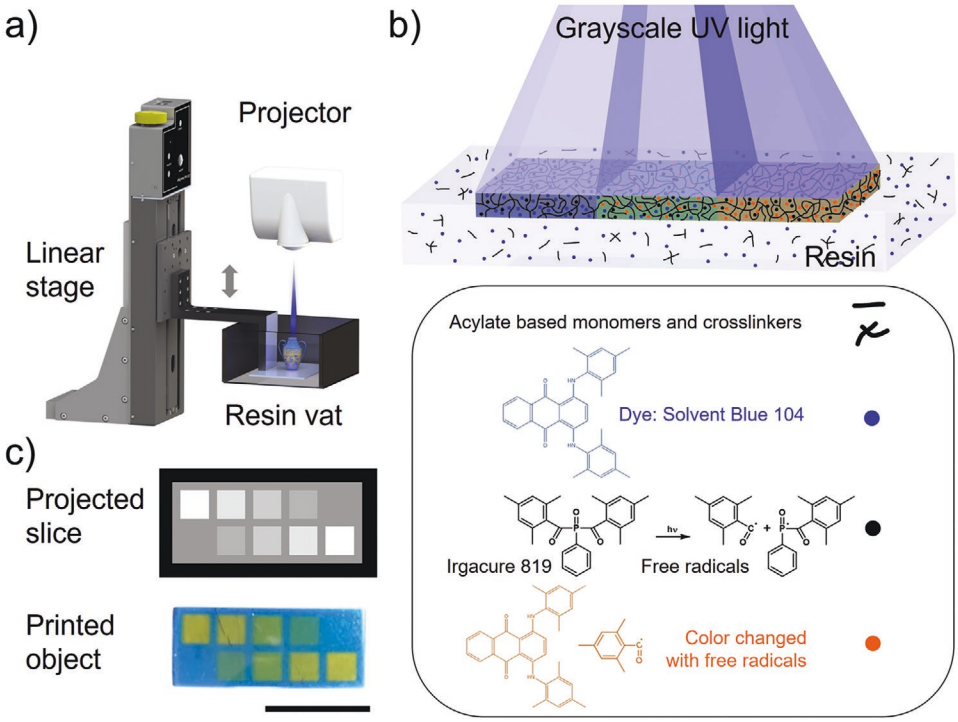

Figure 1. The printing method and mechanism. a) Schematics of the top-down DLP printer. b) Schematics showing the structures and reactions applied in the colored-DLP method. The anthraquinone-based dye (Solvent Blue 104) can be oxidized by the free radicals released from photoinitiators (Irgacure 819) under UV light and change the color from blue to yellow, so that the color of the object can be locally controlled by the grayscale level in the projecting slices during DLP printing. c) The projected grayscale slice and the corresponding printed object with different colors ranging from blue to yellow. Scale bar: 10 mm.

inkjet 3D printers, as multiple nozzles can dispense multiple materials with different colors. By comparison, multi-material DLP printing is intrinsically more difficult owing to the single-batch, single-material characteristic of the vat polymerization mechanism. To overcome this limitation, different strategies have been employed, including selectively initiating independent photo-crosslinking systems,[32,33] tuning the grayscale of the light patterns,[34,35] and replacing the resin by customized devices, such as removable vat equipped with pump,[36] rotating vat carousel,[37] or dynamic fluidic control with integrated fluidic cells.[38] However, these methods either use a single vat with resins of unchangeable color or require sophisticated devices that involve complicated manipulation and cleaning, which severely restrict the efficient fabrication of multi-color 3D prints by DLP.

In this work, we develop a practical and efficient approach for multi-color DLP printing. We successfully print multi-color parts in a single-vat, single-batch manner without post-processing through the combination of a diamino-substitute anthraquinone-based dye (Solvent Blue 104, or SB104) and precise control over the light exposure. Different from other functional dyes used in 3D printing,[39] SB104 exhibits color change in the presence of free radicals. Under UV exposure, the dye can be oxidized by the free radicals released from photo-initiators (Figure 1b), concomitant with a color change from blue to yellow (Figure 1c). The color change shows a strong dependence on the light dose, thus enabling a wide spectrum of colors by controlling the grayscale (or light intensity) of the light pattern or the exposure time in the printing process, needless of extra vats or devices. To precisely encode the color distribution of the samples, we establish the relationship between the light dose and the color of the printed samples. This controllable color change between inverted colors (blue and yellow) provides an informative viridis-style colormap[21,40,41] for various applications. To demonstrate the versatility and efficiency of our multi-color DLP, multi-color demonstrations, such as engineering stress simulation results in 3D, and multi-color vases, are successfully fabricated. This novel strategy can be extended to anthraquinone-based dyes (Figure S1, Supporting Information) with different colors (including red, green, and violet) to further expand the range of colors and find potential applications in the 3D printing industry.

2. Results and Discussion

2.1. Digital Light Process and Materials

A top-down DLP 3D printer is used in this study. As shown in Figure 1a, it consists of a UV light projector (PRO4500, 385 nm, Wintech, San Marcos, CA, USA), a liquid resin vat, and a linear motion stage (LTS150, Thorlabs, Newton, NJ, USA), on which the printing platform is mounted. In the printing process, slices of part cross-section images are projected by the projector to selectively cure the liquid resin on the top surface in the resin vat. Once a layer is cured, the platform goes down

and is immersed by the liquid resin again so that another layer can be printed. In this way, the 3D object can be fabricated layer-by-layer. The entire printing procedure is controlled by a Python program with a graphical user interface (GUI).

Anthraquinone derivatives are extensively used in dyeing and the textile industry, providing a full range of colors covering the visible wavelength band. Anthraquinone is almost colorless with very weak absorption in the visible wavelength range.[42] In the presence of additional electron-donating groups, the bathochromic shift causes significant visible wavelength absorptions due to the charge-transfer transitions with the carbonyl groups.[43] The bathochromic shift increases with the electron-donating abilities of substituents and brings deeper color. However, decolorization happens when the stable charge-transfer state of an anthraquinone-based dye changes. Most dye decolorization is due to oxidation.[44,45] The color of the anthraquinone-based dye changes with the level of oxidation. In DLP printing, the free radical concentration can be locally controlled by modulating the UV light intensity at pixel level. Therefore, it provides a feasible method to locally control the level of the dye oxidation by free radical, thus results in the color change of the dye. To demonstrate this approach, a commercial diamino-substitute anthraquinone-based dye Solvent Blue 104 (SB 104) is selected in this work. The strong amino substituents attribute to the long-wavelength absorption and yield a brilliant blue color. It also possesses a wilder color transition in decolorization. In addition to SB 104, various anthraquinone-based dyes (Figure S1, Supporting Information), such as Disperse Red 9 (red color), Solvent Green 3 (green color), Solvent Violet 13 (violet color), and Solvent Blue 35 (blue color), also exhibit similar yellowing color change with the presence of free radicals, which provide a wide range of colors for various applications.

2.2. Characterizations of the Color Change and Photopolymerization

To characterize the change of color of SB 104, UV–vis absorption spectroscopic analysis is performed. The samples containing the same ingredients (Irgacure 819 0.165 wt% and SB104 0.025 wt%, dissolved in isopropyl alcohol [IPA]) are exposed to a UV light (385 nm, 55 mW cm^{-2}) for 0, 4, 7, 10, 14, 19, and 25 s, respectively. As shown in **Figure 2**a, the samples display a color gradient ranging from blue to yellow. It is noted that oxidation decolorization displays a bathochromic shift from long wavelength to short wavelength (blue [≈430–500 nm] –cyan [≈500–520 nm]–green [≈520–560 nm]–yellow [≈560–580 nm]).[46,47] This agrees with the experimental results shown in Figure 2a. From the absorption spectra in Figure 2b, we can see that with the increase of the time of UV light exposure, the absorptional peaks at about 585 and 635 nm, which show a blue color, diminish gradually. While the absorbance between about 430 to 500 nm, which shows yellow, increases. It is noted that the color change can be realized by free radicals released by other photoinitiators. As an example, another photoinitiator, Irgacure 651, is also characterized. As shown in Figure S2, Supporting Information, the increase of the absorption between ≈430 and 500 nm is more obvious. A wide choice of photoinitiators allows this method to be efficiently applied on a wide range of DLP printers with different UV light sources

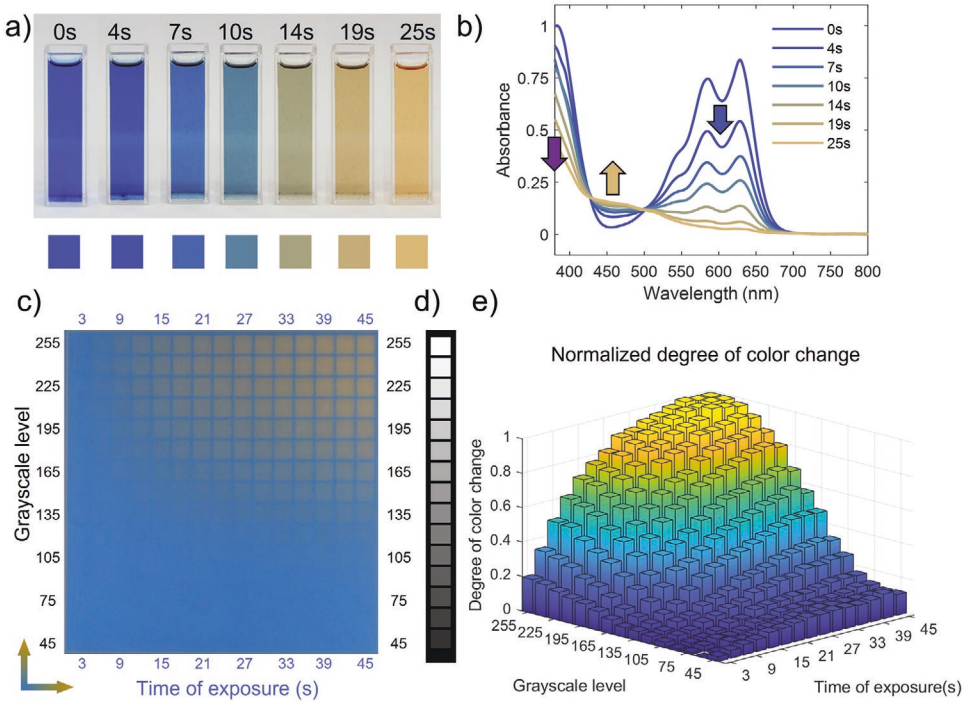

Figure 2. Characterizations of the color change. a) The color change of the solution containing SB104 dye (0.025 wt%) with Irgacure 819 (0.165 wt%) after different time of UV light exposure. b) The UV–vis absorption spectra of the samples shown in (a). c) The color change matrix of the DLP resin under different grayscale levels (GL45-GL255) and time of exposure (3–45 s) to the DLP projector. d) The grayscale figures used in (c). e) Normalized degree of color change obtained from (c).

and different wavelengths. As shown in Video S1, Supporting Information, both Irgacure 819 and Irgacure 651 can intrigue the color change, while Irgacure 819 works more efficiently in the case of 385 nm UV light.

To utilize this color-changing mechanism in DLP 3D printing, we further characterize the color change within the DLP resin system. An ink system containing two acrylate-based monomers (2-hydroxyethyl acrylate and isodecyl acrylate), a diacrylate crosslinker (Ebecryl 8807), the photoinitiator (Irgacure 819), and the blue dye SB104 is made as a demonstration. In this study, 8-bit grayscale images are used for the DLP projection, in which there are 256 grayscale levels (GL) indicating different light intensities. A thin layer of resin is sandwiched between two glass slides by a space (50 μm). Here, we control two variables, that is, the grayscale and the exposure time. Figure 2c shows the results in a 15 by 15 matrix, where the columns vary in exposure time and the rows vary in grayscale value. The grayscale figure projected is shown in Figure 2d with the grayscale levels of GL 45, GL 60, GL 75, ..., GL 240, and GL 255. We can observe that with the increase of either time of exposure or light intensity, the color changes gradually from blue to yellow. To quantify the color change shown in the matrix, the CIELAB color space (International Commission on Illumination, CIE, 1976), also referred to as $L^*a^*b^*$ color space, is adopted.[42–45] Herein, the b^* values of the sample matrix represent the blue-yellow opponents, and are utilized to calculate the color change. We can normalize the degree of color change (DoCC) with the following Equation(1).

$$\mathrm{DoCC} = \frac{b^* - b^*_{\min}}{b^*_{\max} - b^*_{\min}} \times 100\% \tag{1}$$

where $b^*_{\min}$ denotes the b^* value of the sample point with the least light dose, and $b^*_{\max}$ denotes the b^* value with the highest light dose, assuming that the color does not change with the least light dose (DoCC = 0) and fully changes with the highest (DoCC = 1). The DoCC of the sample matrix is plotted in Figure 2e. Similarly, DoCCs are characterized for different printing conditions with different resins and layer thicknesses; the details are provided in Figure S3, Supporting Information. In addition, according to the degree of conversion (DoC) characterized by Fourier transform infrared spectra (FTIR), the color-changing process takes place in a phase later than the photopolymerization process (Figure S4, Supporting Information). Therefore, the change of color does not cause obvious inconsistency in modulus or any loss in tensile strength (Figure S5, Supporting Information).

In addition to color presenting, the dye is also playing another important role in this 3D printing resin system as the photoabsorber, which could help increase the printing resolution in z-direction and obtain fine structures.[35,48,49] The UV light transmittance through the ink and the change of the UV light transmittance during photopolymerization and color change is measured (details provided in Figure S6, Supporting Information). From the plot, we can see that the light transmittance first increases as the light dose increases. This is caused by both the decomposition of the photoinitiator and the changing of color. In the control group, where there is only the same amount of photoinitiator dissolved in IPA, there is also a growing light transmittance with the increasing light dose, which shows the effect of photoinitiator on the light transmittance. In the resin, with the presence of dyes as the photoabsorber, the increase of light transmittance is slower than that of the control groups. Although the light transmittance is gradually changing and the reaction kinetics is complex, we can use an existing model[50–52] (see the Supporting Information for model details) to approximate the curing depth or the position of the curing front. As shown in Figure S6, Supporting Information, the model fits the curing depth data obtained under different grayscale levels very well within the normal light dose range for printing and color change. As the light dose increases, the curing depth first grows fast and then slows down under the limit of the light transmittance in the resin. Therefore, the loss of resolution is limited even though a high light dose might be needed for color change.

In the layer-by-layer printing process, each layer may experience multiple light exposures as a result of the light penetration from the new layers. In extreme cases, in need of yellow unsupported structures like a beam or bridge, over curing may cause a loss of resolution. To investigate this extreme case, yellow bridges with various thicknesses (0.1–0.5 mm) are printed and measured (Figure S7a, Supporting Information). The results show that the loss of resolution in thickness is around 0.224 mm for unsupported thin features, not expanding with the increasing of designed thickness with a growing number of exposures. Due to light penetration, the DoCC is also subject to change with multiple light exposures in the printing process. To investigate the effect of yellow layers over blue layers, we design a wall structure with blue and yellow check patterns embedded. However, even in this extreme case, as shown in Figure S7b–e, Supporting Information, the effect of yellow layers over blue layers is constrained within two layers (100 μm) due to the limited light transmittance (Figure S6a,b, Supporting Information) and high light dose needed for color changing (Figure S4d, Supporting Information).

The dye is not directly involved in the photopolymerization reactions, so it is also generally compatible with other commonly used photopolymer resins. For example, the dye performs very well with polyethylene (glycol) diacrylate (PEGDA) (Mn = 700 g mol^{-1}), which is widely used in 3D printing and biomedical applications.[53] In addition, it is worth noticing that the color-changing rate varies with different polymer networks structures, because the color changing takes place in a phase later than polymerization, and the degree of freedom of radicals in the polymer network is different. In general, longer molecular chains will give more freedom to the color-changing process and allow a higher color-changing speed. To illustrate this, we show the color change of dye within PEGDA with different Mn (250, 575, and 700 g mol^{-1}). The details are provided in Figure S8, Supporting Information, and the results show that the dye in the network formed by PEGDA 700 already changed the color most obviously with the provided light dose, while the color change in that of PEGDA 575 is less obvious, and the color change in that of PEGDA 250 can hardly stand out.

2.3. Colored 3D Terrain Printing

With the relationship of color change as a function of grayscale, we first print the 3D terrain of an island. Herein, the color is utilized as an index of the altitude, and the places of the same

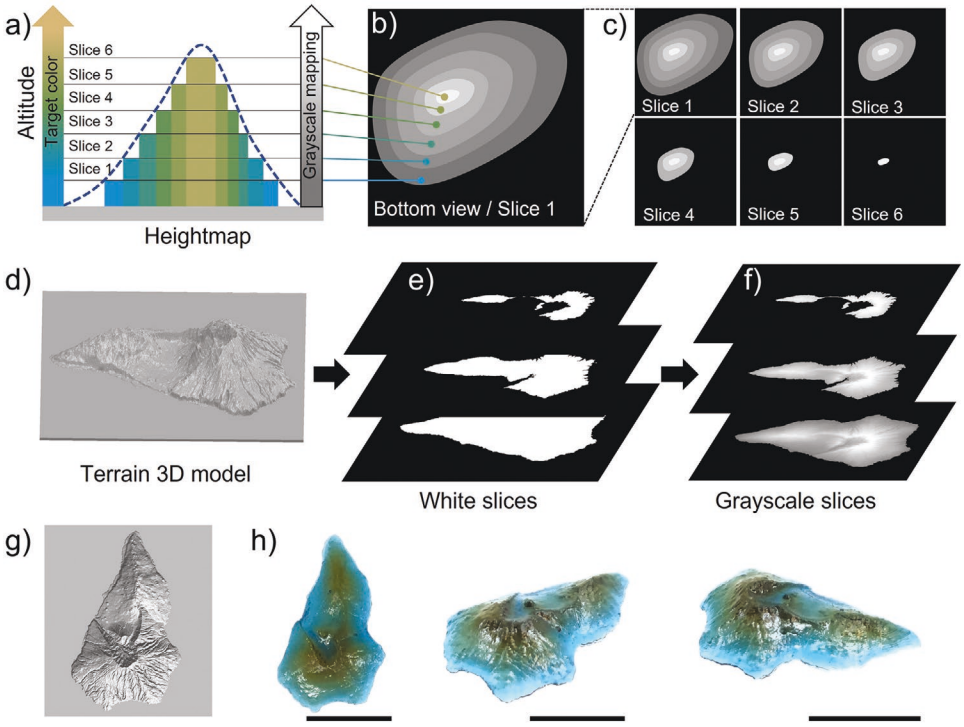

Figure 3. Colored 3D terrain printing. a–c) Schematics showing how to map the altitude to colors and grayscale levels. The target colors are associated with the altitude of the 3D model, and the local grayscale levels in the slices are determined by the computed altitude of the model. The generation of printing slices: d) the 3D model, e) the white slices generated from the model, and f) the processed grayscale slices. g) The comparison between the 3D model and h) the printed object. Scale bars: 10 mm.

altitude are shown by the same color. **Figure 3**a–c shows the strategy to map the altitude to different colors and grayscale levels. The highest part of the landscape is designated to the fully changed color, yellow, which corresponds to the brightest part in the slice (GL 255). The lowest part is designated to the unchanged color, corresponding to the dimmest grayscale level (GL 120). To ensure that the color can be correctly presented from different viewpoints, even with transparent resins, we project the color from upper layers to lower layers, making the inside color identical in the *z*-direction. The procedures of generating the printing slices are shown in Figure 3d–f. The 3D model of the island (in STL format) is first sliced into white slices and then processed with MATLAB to generate the grayscale slices following the above-described strategy. In this demo, the layer thickness is 50 µm, and the curing time for each layer is 24 s. From the printed result (Figure 3h), we can easily recognize the altitude of the landscape through the color presented on the 3D object.

2.4. 3D Visualization of the Engineering Stress Simulation Results

To further demonstrate the ability to spatially distribute the colors as carriers of information, we developed the method to directly print the finite element analysis (FEA) simulation results with our multi-color DLP system. A python script was developed to slice the ODB files in ABAQUS (Dassault System, Providence, RI, USA), one of the most widely used FEA software. As shown in **Figure 4**a–d, we first ran the FEA simulation of a uniaxial tensile test of a sheet with a hole in ABAQUS. In the contour plot of the engineering strain (Figure 4a), we can observe the strain concentration on the edge of the hole. Then we used the Python script to output the grayscale contours of engineering strain in all of the cross-sections in *z*-direction. These cross-sections were cut with a fixed interval, 50 µm, which is the layer thickness in the DLP printing. The output contours were mapped to a suitable range of grayscale level for the DLP printing. Figure 4c,d shows the printed result, which visualizes the stress concentration effect very well in a 3D manner. It is worth noting that the range of grayscale should be optimized for a more gradual change in color, instead of using the full range. Here the grayscale value ranges from GL 90 to GL 255. Comparisons can be found in Figure S9, Supporting Information. Similarly, we also visualize the 3D engineering strain contour in a wrench. In this design, the wrench head is slightly thicker than the shaft. Figure 4e shows the engineering strain contour, and Figure 4f shows the printing slice at the middle plane of the wrench. As shown in Figure 4g, the wrench displays more delicate 3D features than the planar sheet. From the top view in Figure 4h, it can be seen that the contour of the engineering strain is accurately visualized. Unlike traditional methods[54,55] for colored 3D printing of simulation results, this method allows direct printing of simulation results without the need for intermediary files such as VRML or STL files.

2.5. Complex Artistic Printings and Encrypted Printings

To further explore the capabilities of fabricating 3D objects with complex geometries and multiple colors, we design and fabricate

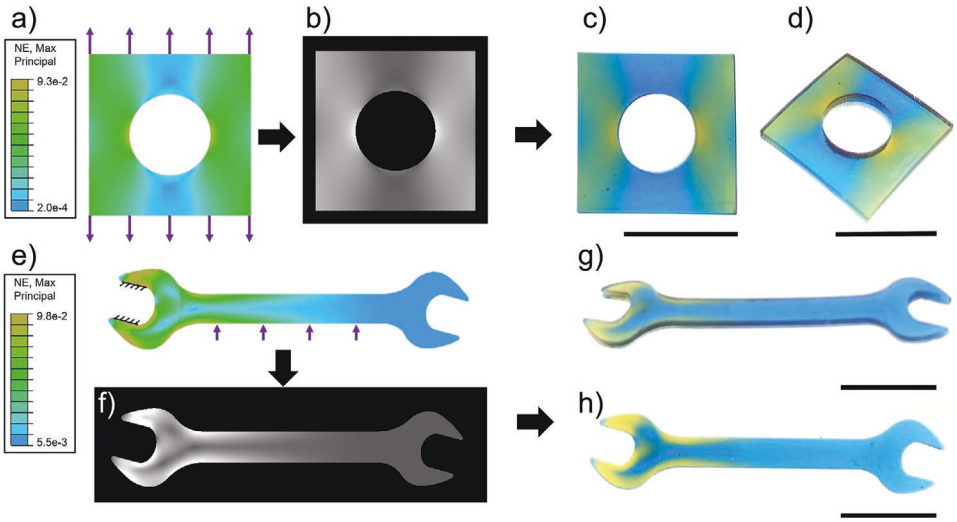

Figure 4. 3D visualization of the simulation results. a–d) A sheet with a whole: the simulation result in ABAQUS, one of the output slices for printing and the printed object. e–h) A wrench: the simulation result in ABAQUS, one of the output slices for printing and the printed object. Scale bars: 10 mm.

a vase with complex artistic multi-color patterns, following a general method for slicing and printing multi-color designs, as shown in **Figure 5**a. In this method, STL parts for different colors are exported from the computer-aided design (CAD) assembly. Then these parts are sliced individually under the fixed coordination. Finally, the slices are combined to generate the grayscale slices in MATLAB. In this complex patterned vase (Figure 5b), the grayscale level for the blue part and the yellow part is set as GL 120 and GL 255, respectively. For each 50 µm layer, the curing time is 24 s. In order to further increase the printing efficiency, we propose a novel strategy to reduce the printing time: we conduct a nonlinear histogram equalization on the slices to make the brightest part of each slice equal GL 255, so that we can use the full power of the DLP projector to change the color as desired within the shortest time of exposure for a certain layer. As an example, sample slices of the vase before and after optimization are shown in Figures 5c and 5d, respectively. The nonlinear histogram equalization is conducted following the DoCC contour, as shown in Figure 5e. The contour is plotted with the information derived from Figure 2e, and each line in the contour represents a set of printing parameters yielding the same DoCC. In the optimization process, we shift the grayscale levels along the lines in the contour of DoCC from a longer time of exposure (24 s) to a shorter time of exposure (3 s). In this way, we obtain a set of new grayscales yielding the same DoCC but using a shorter time of exposure (3 s). As a simple example of this strategy, all slices consisting of only GL 120 (printed as blue), such as slices A, D, and E in Figure 5c, are replaced by figures with the same patterns but a full brightness (GL 255), as shown in Figure 5d. The total time of printing is reduced by 30% for this print. Figure 5f shows the CAD design and the actual printed object, demonstrating a great capability of distributing different colors in a complex geometry in an efficient and voxelated manner.

To further highlight the capabilities of spatially designating different parts of the entire structure to different colors, we fabricate an opaque cube with the opaque resin (see Experimental Section). As shown in Figure 5g, multiple groups of information, including a figure of a yellow jacket and a quick response (QR) code, are embedded into the slices in grayscale. When printed out (time of exposure/layer thickness = 24 s/50 µm), it is hard to tell the difference between the one with the designed patterns and the blank controlled one (Figure S10b, Supporting Information), which has no pattern inside. Due to the same material constituents and high DoC for both blue and yellow parts, one cannot read the information encrypted inside with non-destructive methods, such as computerized tomography (CT) or ultrasonic testing (UT). In order to read the information embedded, the cube is cut, as shown in Figure 5h, and the QR code is scannable. As an addition to the previous DLP encrypting methods,[56] this unique way of information reading ensures that the information is not divulged or accessed before destructive reading, which works like the envelope seal as proof of the privacy of the information.

For the cases where inside color is not used, we develop another method to efficiently make multi-color structures by selective DLP post-curing. We first quickly print the objects using the normal DLP method with our color-changing resin, using a layer thickness of 50 µm and a curing time of 2 s. We then use the DLP projector to selectively post-cure the finished object after cleaning the residual resins. As shown in **Figure 6**a, designed patterns were projected on the preprinted objects from a specific angle. With adequate UV exposure (3 min), the color-changing procedures can still take place in the material. Figure 6b shows the patterns and corresponding multi-color lattices fabricated with this method. After selective post-curing from a diagonal angle for 3 min, the lattices are successfully recolored as designed.

Due to the intrinsic sensitivity of anthraquinone-based dye to environmental oxidation, the programmed colors may be subject to change due to UV exposure or further oxidation. The printed colored sample can be potentially used as a self-integrated indicator for UV exposure time monitoring. However, these unexpected changes could be avoided through protection by applying a UV-resistant coating after printing. In addition, preserving the color without using coating is worth further investigation. Inorganic nanoparticles such as ZnO and TiO_2 have been widely used as blocking agents in transparent UV-resistant coating.[57–59] Organic nanomaterials, such as cellulose nanofiber[60] and dopamine nanoparticles,[61] can also provide highly transparent UV-resistant and antioxidant coating to preserve the printed color. Figure S11,

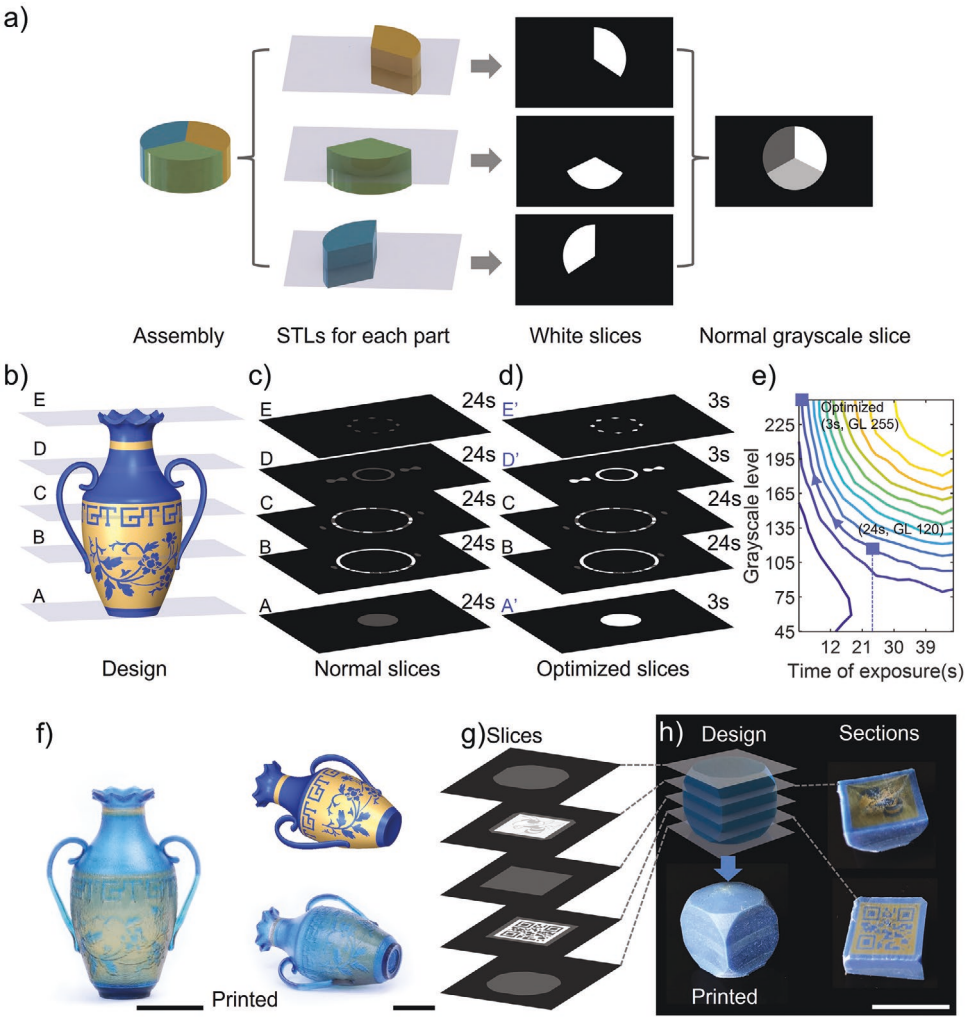

Figure 5. a)The general method of grayscale slicing for multi-color models. b) The design of the vase with artistic patterns and slices after optimization. c) Normal slices before optimization. d) Optimized slices with increased grayscale levels and reduced printing time. e) The DoCC contour for optimization of printing parameters, according to which the printing parameters can be optimized. f) The CAD design and the actual printed object. Complex patterns of the vines with flowers, "GT" characters, are well presented in the printing. g,h) Slices and the printed objects with encryption. The yellow jacket pattern, and scannable QR code is embedded in the printing. Scale bars: 10 mm.

Supporting Information, shows the photo of the sample when the color is freshly programmed and the photo taken after more than 3 months. The sample is sandwiched in glass slides and stored in a cabinet. The colors are well preserved even though there is a small amount of diffusion at the edges of different color checks. The dye molecule will not leak out in the subsequent procedures after printing, including necessary washing with IPA. However, it might be subjected to dilution if soaked in solvents for a long time due to the penetration of the solvent, and the dilution depends on the solvent type, resin material, and the structure size. The mechanism of color change caused by the environment after printing also requires further investigation.

3. Conclusion

In this paper, we present a new approach to realize multi-color 3D printing with a single material via grayscale DLP and a commercial anthraquinone-based dye. The DoCC with different curing times and grayscale levels are characterized, which allows the precise control of the color change in printings and the fabrication of multi-color objects. As demonstrations, methods for 3D printing of colored terrains, visualization of FEA simulation results, fabrication of complex artistic multi-color designs, selective post-curing of surficial color, and encryption of information with inside color are presented, showing a great potential in the area of art, education, engineering visualization, and cyber security.

4. Experimental Section

Transparent Resin: 30 wt% of aliphatic urethane diacrylate (Ebecryl 8807; Allnex, Alpharetta, GA, USA) crosslinker, 50 wt% of 2-hydroxyethyl acrylate (HEA; Sigma-Aldrich, St. Louis, MO, USA) monomer, and 19 wt% of isodecyl acrylate (IA; Sigma-Aldrich) monomer were first mixed. Then 4 wt% of phenylbis (2,4,6-trimethylbenzoyl) phosphine oxide (Irgacure 819, Sigma-Aldrich) and 0.06 wt% of 1,4-Bis(mesitylamino) anthraquinone (Solvent Blue 104, Clariant Corp., Frankfurt, Germany)

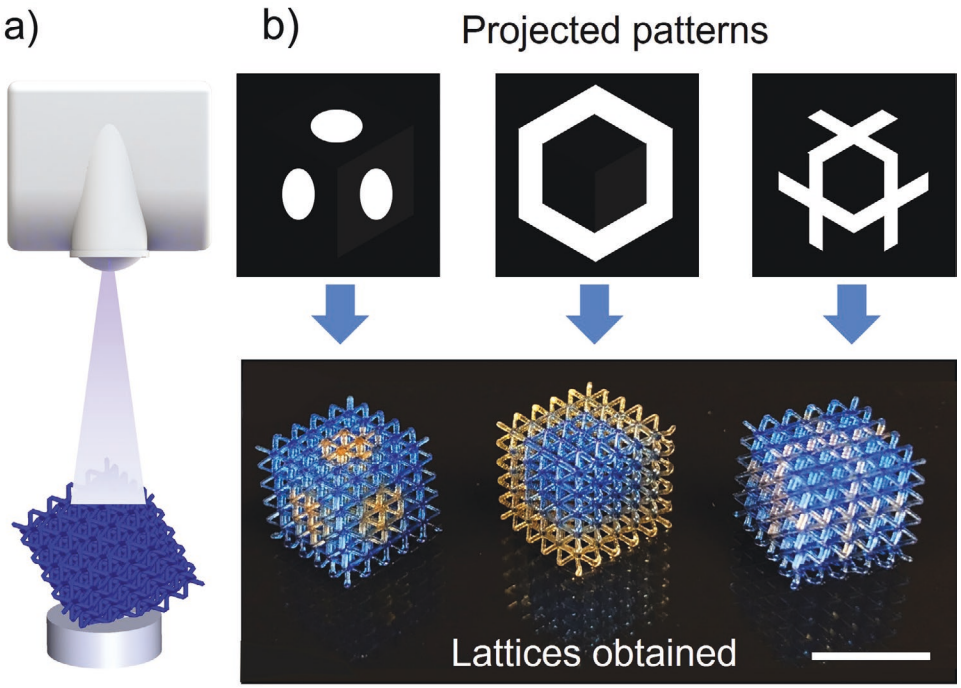

Figure 6. Multi-color structures by selective DLP post-curing. a) The post-curing schematic figure of the selective post-curing method for changing the superficial color. b) The projected patterns and processed lattices through selective post-curing. Scale bar: 10 mm.

were added into the mixture for photoinitiating and color changing. The viscosity of the elastomer ink was low enough for DLP printing.

Opaque Resin: To prepare the opaque resin, the transparent resin and the white pigment (TiO_2 nanopowder, rutile phase, average size 200 nm, Inframat Corporation, Manchester, CT, USA) were mixed at a mass ratio of 98.5%:1.5%.

DLP Slice Preparation: To prepare the files for general printing as shown in Figure 5a, the CAD model assembly, including parts with different colors, was first designed in SOLIDWORKS 2019 (Dassault Systèmes, Velizy-Villacoublay, France) and exported as STL files. Then, these STL files were sliced into white 2D images separately using CreationWorkshop software (DaraTree3D, Dallas, TX, USA). Finally, the white images were processed by MATLAB (MathWorks, Natick, MA, USA) codes to generate the grayscale images.

Light Intensity: The light intensity of the projector was measured by an ILT1400-A Radiometer Photometer (International Light Technologies Inc., Peabody, MA, USA).

UV–Vis Spectroscopy: UV–vis absorption spectroscopy was performed with a spectrometer (Model 8453, Agilent Technologies Inc., Santa Clara, CA, USA). IPA (Sigma-Aldrich) was used as the solvent for all samples. The spectral resolution was 1 nm over the spectral region of interest. The raw data are smoothed using a Gaussian filter of size 20 in MATLAB, and then shifted at 890 nm for baseline correction. The whole data set was normalized by its maximum intensity value at 370–800 nm.

Fourier Transform Infrared Spectra: FTIR spectra (Nicolet iS50 spectrometer, Thermo Fisher Scientific, Waltham, MA) were obtained by averaging 32 scans of the signal at a resolution of 2 cm^{-1} in attenuated total reflectance mode.

Pre-Processing of DoCC Characterization: The JPG picture of the resin sample from the camera was cropped to keep the testing area only. In MATLAB, for each one of the 15 by 15 testing points, the RGB value was obtained by averaging a 30-pixels-by-30-pixels area. The RGB values were then converted to CIELAB color space for further calculation and plotting of DoCC.

Statistical Analysis: Error bars in the plots indicated the standard deviation over at least four tests on the specimens. Two-sample *t*-test was used to assess the significance of the difference of mechanical properties between the blue and yellow 3D printed parts. The results did not reject the null hypothesis that the two groups had the same mean values at the 0.05 significance level, and the *p* values were 0.072 and 0.5414 for the modulus and tensile strength, respectively. All data were processed using MATLAB.

Supporting Information

Supporting Information is available from the Wiley Online Library or from the author.

Acknowledgements

This work was supported by an NSF grant (1931977) and an AFOSR grant (FA 9550-20-1-0306; Dr. B.-L. "Les" Lee, Program Manager), the gift funds from HP Inc. and Northrop Grumman Corporation. This work was performed in part at the Georgia Tech Institute for Electronics and Nanotechnology, a member of the National Nanotechnology Coordinated Infrastructure, which is supported by the National Science Foundation (ECCS-1542174).

Conflict of Interest

X.P., H.J.Q., L.Y., and C.-M.C. are inventors on a provisional patent application related to this work filed by Georgia Tech Research Corporation (US no. 63/327,997, filed on 6th April 2022). The authors declare that they have no other competing interests.

Data Availability Statement

The data that support the findings of this study are available from the corresponding author upon reasonable request.

Keywords

additive manufacturing, digital light processing, grayscale digital light processing, multi-color 3D printing

Received: December 6, 2021
Revised: March 9, 2022
Published online: April 15, 2022

[1] I. Gibson, D. Rosen, B. Stucker, M. Khorasani, in *Additive Manufacturing Technologies*, 3rd ed. Springer International Publishing, Cham **2021**, p. 23.
[2] S. C. Ligon, R. Liska, J. Stampfl, M. Gurr, R. Mülhaupt, *Chem. Rev.* **2017**, *117*, 10212.
[3] B. Berman, *Bus. Horiz.* **2012**, *55*, 155.
[4] S. Tibbits, *Archit. Des.* **2014**, *84*, 116.
[5] Q. Ge, H. J. Qi, M. L. Dunn, *Appl. Phys. Lett.* **2013**, *103*, 131901.
[6] Q. Ge, C. K. Dunn, H. J. Qi, M. L. Dunn, *Smart Mater. Struct.* **2014**, *23*, 094007.
[7] A. S. Gladman, E. A. Matsumoto, R. G. Nuzzo, L. Mahadevan, J. A. Lewis, *Nat. Mater.* **2016**, *15*, 413.
[8] Z. Ding, C. Yuan, X. Peng, T. Wang, H. J. Qi, M. L. Dunn, *Sci. Adv.* **2017**, *3*, e1602890.
[9] X. Kuang, D. J. Roach, J. Wu, C. M. Hamel, Z. Ding, T. Wang, M. L. Dunn, H. J. Qi, *Adv. Funct. Mater.* **2019**, *29*, 1805290.
[10] X. Zheng, H. Lee, T. H. Weisgraber, M. Shusteff, J. Deotte, E. B. Duoss, J. D. Kuntz, M. M. Biener, Q. Ge, J. A. Jackson, S. O. Kucheyev, N. X. Fang, C. M. Spadaccini, *Science* **2014**, *344*, 1373.
[11] M. Kadic, G. W. Milton, M. Van Hecke, M. Wegener, *Nat. Rev. Phys.* **2019**, *1*, 198.
[12] S. M. Montgomery, X. Kuang, C. D. Armstrong, H. J. Qi, *Curr. Opin. Solid State Mater. Sci.* **2020**, *24*, 100869.
[13] S. Derakhshanfar, R. Mbeleck, K. Xu, X. Zhang, W. Zhong, M. Xing, *Bioact. Mater.* **2018**, *3*, 144.
[14] Q. Yan, H. Dong, J. Su, J. Han, B. Song, Q. Wei, Y. Shi, *Engineering* **2018**, *4*, 729.
[15] J. Li, C. Wu, P. K. Chu, M. Gelinsky, *Mater. Sci. Eng. R Rep.* **2020**, *140*, 100543.
[16] S. J. Leigh, R. J. Bradley, C. P. Purssell, D. R. Billson, D. A. Hutchins, *PLoS One* **2012**, *7*, e49365.
[17] Q. Mu, L. Wang, C. K. Dunn, X. Kuang, F. Duan, Z. Zhang, H. J. Qi, T. Wang, *Addit. Manuf.* **2017**, *18*, 74.
[18] H. W. Tan, J. An, C. K. Chua, T. Tran, *Adv. Electron. Mater.* **2019**, *5*, 1800831.
[19] J. R. Tumbleston, D. Shirvanyants, N. Ermoshkin, R. Janusziewicz, A. R. Johnson, D. Kelly, K. Chen, R. Pinschmidt, J. P. Rolland, A. Ermoshkin, E. T. Samulski, J. M. Desimone, *Science* **2015**, *347*, 1349.
[20] D. A. Walker, J. L. Hedrick, C. A. Mirkin, *Science* **2019**, *366*, 360.
[21] F. Crameri, G. E. Shephard, P. J. Heron, *Nat. Commun.* **2020**, *11*, 5444.
[22] C. Liu, B. Qian, R. Ni, X. Liu, J. Qiu, *RSC Adv.* **2018**, *8*, 31564.
[23] S. R. Petersen, J. A. Wilson, M. L. Becker, *Macromolecules* **2018**, *51*, 6202.
[24] I. Roppolo, F. Frascella, M. Gastaldi, M. Castellino, B. Ciubini, C. Barolo, L. Scaltrito, C. Nicosia, M. Zanetti, A. Chiappone, *Polym. Chem.* **2019**, *10*, 5950.
[25] P. Punpongsanon, X. Wen, D. S. Kim, S. Mueller, in *Proceedings of the 2018 CHI Conference on Human Factors in Computing Systems*, **2018**, p. 1.
[26] Y. Jin, I. Qamar, M. Wessely, A. Adhikari, K. Bulovic, P. Punpongsanon, S. Mueller, in *Proceedings of the 32nd Annual ACM Symposium on User Interface Software and Technology*, **2019**, pp. 701–712.
[27] M. Boulaala, D. Elmessaoudi, I. Buj-Corral, J. El Mesbahi, O. Ezbakhe, A. Astito, M. El Mrabet, A. El Mesbahi, *Int. J. Adv. Manuf. Technol.* **2020**, *110*, 45.
[28] M. A. Skylar-Scott, J. Mueller, C. W. Visser, J. A. Lewis, *Nature* **2019**, *575*, 330.
[29] K. Van Wieren, H. N. Tailor, V. F. Scalfani, N. Merbouh, *J. Chem. Educ.* **2017**, *94*, 964.
[30] X. Peng, X. Kuang, D. J. Roach, Y. Wang, C. M. Hamel, C. Lu, H. J. Qi, *Addit. Manuf.* **2021**, *40*, 101911.
[31] B. B. Patel, D. J. Walsh, D. H. Kim, J. Kwok, B. Lee, D. Guironnet, Y. Diao, *Sci. Adv.* **2020**, *6*, eaaz7202.
[32] N. D. Dolinski, Z. A. Page, E. B Callaway, F. Eisenreich, R. V. Garcia, R. Chavez, D. P. Bothman, S. Hecht, F. W. Zok, C. J. Hawker, *Adv. Mater.* **2018**, *30*, 1800364.
[33] J. J. Schwartz, A. J. Boydston, *Nat. Commun.* **2019**, *10*, 791.
[34] G. I. Peterson, J. J. Schwartz, D. Zhang, B. M. Weiss, M. A. Ganter, D. W. Storti, A. J. Boydston, *ACS Appl. Mater. Interfaces* **2016**, *8*, 29037.
[35] X. Kuang, J. Wu, K. Chen, Z. Zhao, Z. Ding, F. Hu, D. Fang, H. J. Qi, *Sci. Adv.* **2019**, *5*, eaav5790.
[36] J.-W. Choi, E. Macdonald, R. Wicker, *Int. J. Adv. Manuf. Technol.* **2009**, *49*, 543.
[37] J.-W. Choi, H.-C. Kim, R. Wicker, *J. Mater. Process. Technol.* **2011**, *211*, 318.
[38] D. Han, C. Yang, N. X. Fang, H. Lee, *Addit. Manuf.* **2019**, *27*, 606.
[39] M. Gastaldi, F. Cardano, M. Zanetti, G. Viscardi, C. Barolo, S. Bordiga, S. Magdassi, A. Fin, I. Roppolo, *ACS Mater. Lett.* **2020**, *3*, 1.
[40] R. Bujack, T. L. Turton, F. Samsel, C. Ware, D. H. Rogers, J. Ahrens, *IEEE Trans. Vis. Comput. Graph.* **2017**, *24*, 923.
[41] J. R. Nuñez, C. R. Anderton, R. S. Renslow, *PLoS One* **2018**, *13*, e0199239.
[42] M. Hattori, U. b. Staff, in *Kirk-Othmer Encyclopedia of Chemical Technology*, **2014**, p. 1.
[43] J. Salabert, R. M. Sebastián, A. Vallribera, *Chem. Commun.* **2015**, *51*, 14251.
[44] E. Routoula, S. V. Patwardhan, *Environ. Sci. Technol.* **2020**, *54*, 647.
[45] S. Jeremić, A. Amić, M. Stanojević-Pirković, Z. Marković, *Org. Biomol. Chem.* **2018**, *16*, 1890.
[46] D. Jacquemin, E. Brémond, I. Ciofini, C. Adamo, *J. Phys. Chem. Lett.* **2012**, *3*, 468.
[47] J. Salabert, R. M. Sebastián, A. Vallribera, *Chem. Commun.* **2015**, *51*, 14251.
[48] Y. Yang, Y. Zhou, X. Lin, Q. Yang, G. Yang, *Pharmaceutics* **2020**, *12*, 207.
[49] Q. Zhang, X. Peng, S. Weng, R. Zhang, D. Fang, R. Zhao, H. J. Qi, *Extreme Mech. Lett.* **2020**, *39*, 100824.
[50] J. T. Cabral, J. F. Douglas, *Polymer* **2005**, *46*, 4230.
[51] A. Vitale, M. G. Hennessy, O. K. Matar, J. T. Cabral, *Macromolecules* **2014**, *48*, 198.
[52] J. Wu, Z. Zhao, C. M. Hamel, X. Mu, X. Kuang, Z. Guo, H. J. Qi, *J. Mech. Phys. Solids* **2018**, *112*, 25.
[53] A. Bagheri, J. Jin, *ACS Appl. Polym. Mater.* **2019**, *1*, 593.
[54] S. Killi, A. Morrison, *Int. J. Mech. Syst. Eng.* **2016**, *2*, 7.
[55] G. C. Onwubolu, *Introduction to SolidWorks: A Comprehensive Guide with Applications in 3D Printing*, CRC Press, Boca Raton, FL **2017**.
[56] F. Mayer, S. Richter, J. Westhauser, E. Blasco, C. Barner-Kowollik, M. Wegener, *Sci. Adv.* **2019**, *5*, eaau9160.
[57] W. Johansson, A. Peralta, B. Jonson, S. Anand, L. Österlund, S. Karlsson, *Front. Mater.* **2019**, *6*, 259.
[58] E. Olson, Y. Li, F.-Y. Lin, A. Miller, F. Liu, A. Tsyrenova, D. Palm, G. W. Curtzwiler, K. L. Vorst, E. Cochran, S. Jiang, *ACS Appl. Mater. Interfaces* **2019**, *11*, 24552.
[59] J. Xu, H. Nagasawa, M. Kanezashi, T. Tsuru, *ACS Appl. Mater. Interfaces* **2018**, *10*, 42657.
[60] K. Kriechbaum, L. Bergström, *Biomacromolecules* **2020**, *21*, 1720.
[61] Y. Wang, J. Su, T. Li, P. Ma, H. Bai, Y. Xie, M. Chen, W. Dong, *ACS Appl. Mater. Interfaces* **2017**, *9*, 36281.